Histol Histopathol (2023) 38: 1295-1306

Histology and Histopathology
From Cell Biology to Tissue Engineering

ORIGINAL ARTICLE Open Access

Hsa_circ_0072765 knockdown inhibits proliferation, activation and migration in transforming growth factor-beta (TGF-β)-induced hepatic stellate cells (HSCs) by the miR-197-3p/TRPV3 axis

Yan Jin, Xueyan Guo, Rong Zhang and Chunying Yan

Department of Gastroenterology, Shaanxi Provincial People's Hospital, Xi'an City, Shaanxi, China

Summary. Background. Circular RNAs (circRNAs) participate in the progression of diverse human diseases. However, the effects of circRNAs on liver fibrosis are limited. In this study, we aimed to investigate the functions of hsa_circ_0072765 in liver fibrosis.

Methods. Transforming growth factor-beta (TGF-β)-treated hepatic stellate cells (HSCs) were used as the cell model of liver fibrosis. Quantitative real-time polymerase chain reaction (qRT-PCR) or western blot was performed to determine the expression of hsa_circ_0072765, microRNA-197-3p (miR-197-3p) and transient receptor potential cation channel subfamily V member 3 (TRPV3). 5'-ethynyl-2'-deoxyuridine (EdU) assay, flow cytometry analysis and wound-healing assay were conducted to evaluate cell proliferation, cell cycle and migration. HSC activation was assessed by determining the expression of alpha-smooth muscle actin (α-SMA) and type I collagen alpha 1 (Col1A1). Dual-luciferase reporter assay and RNA immunoprecipitation (RIP) were manipulated to analyze the relationship of hsa_circ_0072765, miR-197-3p and TRPV3. The exosome morphology was observed under transmission electron microscopy (TEM).

Results. Hsa_circ_0072765 level was increased in TGF-β-induced HSCs. Hsa_circ_0072765 knockdown inhibited cell proliferation, cell cycle, activation and migration in TGF-β-induced HSCs. Hsa_circ_0072765 sponged miR-197-3p and negatively regulated miR-197-3p expression. MiR-197-3p inhibition reversed the effects of hsa_circ_0072765 knockdown on TGF-β-induced HSC proliferation, cell cycle, activation and migration. In addition, TRPV3 was the target gene of miR-197-3p and miR-197-3p overexpression inhibited TGF-β-treated HSC proliferation, cell cycle, activation and migration by targeting TRPV3. Besides, we found that exosomal hsa_circ_0072765 was increased in TGF-β-treated HSCs.

Conclusion. Hsa_circ_0072765 promoted the progression of TGF-β-treated HSCs by decoying miR-197-3p and upregulating TRPV3

Key words: HSCs, TGF-β, hsa_circ_0072765, miR-197-3p, TRPV3

Corresponding Author: Xueyan Guo, Department of Gastroenterology, Shaanxi Provincial People's Hospital, No. 256 West Youyi Road, Xi'an, Shaanxi, 710068, China. e-mail: mothguoxy@126.com

www.hh.um.es. DOI: 10.14670/HH-18-586

Introduction

Liver fibrosis is not an independent disease, but is associated with liver diseases of various sources such as hepatitis virus infection, alcohol abuse, or non-alcoholic steatohepatitis (Lu et al., 2003; Hernandez-Gea and Friedman, 2011). Liver fibrosis is an indispensable part in the progression of chronic liver disease. If not treated in time, a large number of fibrous tissue hyperplasia will occur in the liver, and then the liver fibrosis will develop into cirrhosis, which ultimately poses a serious threat to the life and health of patients (Luersen et al., 2015; Barnett, 2018). Hepatic stellate cells (HSCs) are usually stationary and have irregular characteristics (Matsuda et al., 2018). Under conditions of external stimulation and liver injury, HSCs can be activated and transformed into myofibroblast-like cells, which play an important role in the process of liver fibrosis (Friedman, 2008). However, the activation mechanism of HSCs is still unclear and needs to be further explored.

The non-coding RNAs (ncRNAs), such as microRNAs (miRNAs) and circular RNAs (circRNAs), have been reported to be involved in the development of diverse human diseases (Esteller, 2011; Beermann et al., 2016). CircRNAs possess covalently closed loop structures and can serve as miRNA sponges to regulate target gene expression (Salzman, 2016; Chen et al., 2019). CircRNAs have been testified to be related to

liver diseases (Zeng et al., 2021). For example, circUBAP2 promoted the malignancy of hepatocellular carcinoma (HCC) (Yu et al., 2021). Hsa_circ_0008537 aggravated the carcinogenesis of liver cancer via the miR-153-3p/MCL1 axis and miR-153-3p/Snail1 axis (Yang et al., 2021). Hsa_circ_0072765 is located at chr5: 68471223-68471364 and is formed by CCNB1 gene. A previous study had shown that hsa_circ_0072765 was aberrantly increased in fibrotic liver tissues (Liu et al., 2019). However, the exact roles of hsa_circ_0072765 in liver fibrosis development are unclear.

MiRNAs are small ncRNAs that are related to human disorders, including liver fibrosis (Vishnoi and Rani, 2017). For instance, miR-195-3p contributed to liver fibrosis and HSC activation by interacting with PTEN (Wang et al., 2021). MiR-571 facilitated HSC proliferation and migration and inhibited apoptosis by altering the Notch3 pathway (Cong et al., 2021). Previous studies have reported that miR-197-3p was abnormally expressed in chronic hepatitis C patients and primary biliary cirrhosis patients (Ninomiya et al., 2013; Cabral et al. 2020). However, the relation between miR-197-3p and liver fibrosis is barely known.

Here, we selected hsa_circ_0072765 as the object to reveal its role in the process of liver fibrosis. In this study, the cell model of liver fibrosis was established by treating HSCs with transforming growth factor-beta (TGF-β). Then the functions and mechanisms of hsa_circ_0072765 in TGF-β-induced HSC progression were explored.

Materials and methods

Cell culture and treatment

The HSCs (LX2 cells) were purchased from Procell (Wuhan, China) and cultured at 37°C in DMEM (Procell) supplemented with 10% FBS (Procell) and 1% penicillin/streptomycin (Procell) in an atmosphere containing 5% CO_2.

Hepatic stellate cell line LX2 was used for generating the model for liver fibrosis using TGF-β1. For TGF-β1 treatment, LX2 cells were treated with 5 ng/mL or 10 ng/mL TGF-β1 (Solarbio, Beijing, China) for 24h. To induce the cell model of liver fibrosis, LX2 cells were stimulated with 5 ng/mL TGF-β1 for 24h.

Quantitative real-time polymerase chain reaction (qRT-PCR)

Total RNA was extracted from LX2 cells via the usage of TRIzol reagent (Invitrogen, Carlsbad, CA, USA). The RNAs were then reversely transcribed into cDNAs using the M-MLV (Promega, Madison, WI, USA) for circRNAs and mRNAs or TaqMan MiRNA Reverse Transcriptase Reagent (Vazyme, Nanjing, China) for miRNAs. Subsequently, the qRT-PCR was executed using AceQ Universal SYBR qPCR Master Mix (Vazyme). The results were calculated with the $2^{-\Delta\Delta Ct}$ method. GAPDH and U6 served as the internal controls. The primers are exhibited in Table 1.

Subcellular fraction analysis

This assay was used to explore the distribution of hsa_circ_0072765 in the nuclear and cytoplasmic fractions of LX2 cells. The PARIS Kit (Life Technologies, Grand Island, NY, USA) was used to separate the nuclear and cytoplasmic fractions from LX2 cells according to the manufacturers' instructions. 18S rRNA and U6 were utilized as the controls for cytoplasmic transcript and nuclear transcript, respectively.

RNase R assay

RNase R assay was used to confirm the resistance of hsa_circ_0072765 on RNase R. Total RNA in LX2 cells was treated with or without RNase R (1 U/mg; Epicenter Biotechnologies, Madison, WI, USA) for 20 min and then subjected to qRT-PCR for hsa_circ_0072765 and CCNB1 expression levels.

Actinomycin D assay

Actinomycin D assay was used to explore the stability of hsa_circ_0072765. LX2 cells were exposed to Actinomycin D (Sigma-Aldrich, St. Louis, MO, USA) for 0h, 4h, 8h, 12h and 24h. Then qRT-PCR was executed to determine the expression of hsa_circ_0072765 and CCNB1 in LX2 cells.

Cell transfection

The small interfering RNA against hsa_circ_0072765 (si-hsa_circ_0072765#1, si-hsa_circ_0072765#2, si-hsa_circ_0072765#3) and related negative control si-NC, hsa_circ_0072765

Table 1. Primers sequences used for qRT-PCR.

Name	Primers for PCR (5'-3')	
hsa_circ_0072765	Forward	GCAGCAGGAGCTTTTTGCTT
	Reverse	GCACCATGTCATAGTCCAACA
CCNB1	Forward	TGCAGCACCTGGCTAAGAAT
	Reverse	TAGCATGCTTCGATGTGGCA
miR-197-3p	Forward	GCCGAGTTCACCACCTTCTC
	Reverse	CTCAACTGGTGTCGTGGAG
TRPV3	Forward	CCTCGGATCTGCAGTCCATC
	Reverse	ACCCCGCGTATAGTAGAGCA
GAPDH	Forward	GACAGTCAGCCGCATCTTCT
	Reverse	GCGCCCAATACGACCAAATC
U6	Forward	CTCGCTTCGGCAGCACA
	Reverse	AACGCTTCACGAATTTGCGT
18S rRNA	Forward	CAGCCACCCGAGATTGAGCA
	Reverse	TAGTAGCGACGGGCGGTGTG

overexpression vector (hsa_circ_0072765) and its negative control (circ-NC), miR-197-3p mimic and inhibitor (miR-197-3p and anti-miR-197-3p) and their negative controls (NC and anti-NC), TRPV3 overexpression vector (TRPV3) and control vector (vector) were all provided by GenePharma (Shanghai, China). The cell transfection was conducted by using Lipofectamine 2000 (Invitrogen).

5'-ethynyl-2'-deoxyuridine (EdU) assay

To determine LX2 cell proliferation ability, the EdU detection reagent (Ribibio, Guangzhou, China) was employed. Briefly, LX2 cells cultured in 24-well plates were incubated with EdU for 2h. The cells were immobilized with 4% paraformaldehyde (Sigma-Aldrich), washed with PBS, permeabilized with 0.5% Triton-X-100 (Sigma-Aldrich) and then stained with DAPI (Sigma-Aldrich). The images were observed under a fluorescence microscope (Olympus, Tokyo, Japan) and EdU-positive cells were analyzed.

Flow cytometry analysis

Cell cycle was analyzed using flow cytometry. The LX2 cells were collected, rinsed in PBS and fixed with 4% paraformaldehyde (Sigma-Aldrich). Next, the cells were suspended and stained with propidium iodide (PI; Vazyme) for 20 min in the dark. The cell cycle distribution was analyzed by flow cytometry (BD Biosciences, San Jose, CA, USA).

Western blot assay

LX2 cells were lysed in RIPA buffer (Beyotime, Shanghai, China) to obtain the proteins. The proteins were separated through 10% SDS-PAGE gel and blotted onto PVDF membranes. The membranes were then blocked in 5% skim milk for 2h, incubated with primary antibodies overnight and secondary antibody for 2h. The protein bands were visualized by the ECL system (Beyotime). The primary antibodies Cyclin D1 (bs-0623R), cyclin-dependent kinase 4 (CDK4; bs-0633R), alpha-smooth muscle actin (α-SMA; bs-10196R), type I collagen alpha 1 (Col1A1; bs-10423R) and GAPDH (bs-0755R) and secondary antibody (bs-40295G-HRP) were purchased from Bioss (Beijing, China). The primary antibody against TRPV3 (ab231150) was purchased from Abcam (Cambridge, MA, USA).

Wound-healing assay

To evaluate cell migration ability, wound-healing assay was performed. LX2 cells were seeded into 12-well plates. After 24h, the scratch was created using a pipette tip. The scratch width was recorded at 0h and 24h. ImageJ software was used for the calculation of the area. Wound healing rate was determined according to the following equation: [(the wound area at 0h - the wound area at 24h)/the wound area at 0h] ×100%.

Dual-luciferase reporter assay

This assay was used to confirm the interaction between miR-197-3p and hsa_circ_0072765 or TRPV3. The sequences of wild-type (WT) hsa_circ_0072765 or TRPV3 3'UTR containing the binding sites of miR-197-3p were generated and introduced into pmirGLO (Promega), establishing hsa_circ_0072765-wt and TRPV3-wt. However, hsa_circ_0072765-mut and TRPV3-mut were constructed by mutating the binding sites. The generated vectors were transfected into LX2 cells together with miR-197-3p/NC. 48h later, the luciferase intensity was examined by dual-luciferase reporter assay reagent (Promega).

RNA immunoprecipitation (RIP) assay

RIP assay was performed to further reveal the interaction between between miR-197-3p and hsa_circ_0072765 or TRPV3. The Magna RIP™ RNA Binding Protein Immunoprecipitation reagent (Millipore, Bedford, MA, USA) was employed for RIP assay. In short, LX2 cells were lysed in RIP buffer and cell lysis was incubated with the magnetic beads conjugated with antibody IgG or Ago2. The immunoprecipitated RNA expression was determined.

Exosome isolation and identification

LX2 cells were centrifuged for 10 min at 300×g, the cell supernatants were collected. Then the exosomes were obtained after a series of centrifugations. Briefly, cell medium was centrifuged for 10 min at 2,000g, then for 30 min at 10,000 g to remove any cell debris. Next, the supernatant underwent another centrifugation at 140,000g for 2h to collect the precipitate. The exosomes were suspended in PBS and preserved at -80°C. The morphology of exosomes was observed under transmission electron microscopy (TEM).

To identify the exosomes, the exosome markers CD9 (ab223052; Abcam) and CD63 (ab134045; Abcam) were measured via western blot.

Statistical analysis

All data were obtained from three independent experiments. Data analysis was conducted through GraphPad Prism 7. The data were presented as mean ± SD. Student's *t*-test or one-way ANOVA was utilized for difference analysis. $P<0.05$ was considered as significant.

Results

Hsa_circ_0072765 level was increased in TGF-β1-induced HSCs

LX2 cells were treated with different concentrations of TGF-β1 (0, 5 and 10 ng/mL) for 24h. The results of qRT-PCR showed that hsa_circ_0072765 level was increased in TGF-β1-treated LX2 cells (Fig. 1A).

Moreover, our results showed that hsa_circ_0072765 was mainly enriched in the cytoplasm of LX2 cells rather than the nucleus (Fig. 1B). RNase R assay showed that hsa_circ_0072765 level was not affected by RNase R treatment, but CCNB1 mRNA level was markedly reduced after RNase R treatment (Fig. 1C). Actinomycin D assay indicated that the half-life of hsa_circ_0072765 was longer than CCNB1 in LX2 cells after Actinomycin D treatment (Fig. 1D). All these results indicated that hsa_circ_0072765 was more stable than linear CCNB1, and it was overexpressed in TGF-β1-treated HSCs.

Hsa_circ_0072765 knockdown inhibited the proliferation, cell cycle, activation and migration in TGF-β1-treated HSCs

To explore the functions of hsa_circ_0072765, we constructed si-hsa_circ_0072765#1, si-hsa_circ_0072765#2 and si-hsa_circ_0072765#3 and transfected them into LX2 cells to knock down hsa_circ_0072765 expression. The results of qRT-PCR assay showed that si-hsa_circ_0072765#1, si-hsa_circ_0072765#2 or si-hsa_circ_0072765#3 transfection significantly reduced hsa_circ_0072765 expression LX2 cells compared to si-NC transfected cells (Fig. 2A). LX2 cells with si-hsa_circ_0072765#1 transfection and 5 ng/mL TGF-β1 treatment were utilized for further experiments. EdU assay showed that hsa_circ_0072765 knockdown repressed the proliferation of TGF-β1-treated LX2 cells in comparison with si-NC control group (Fig. 2B). Flow cytometry analysis showed that hsa_circ_0072765 interference inhibited cell cycle process in TGF-β1-activated LX2 cells (Fig. 2C). Moreover, we determined the levels of cell cycle-associated proteins (Cyclin D1 and CDK4) in TGF-β1-treated LX2 cells after si-hsa_circ_0072765#1 transfection. The results exhibited that hsa_circ_0072765 silencing notably reduced the protein levels of Cyclin D1 and CDK4 in TGF-β1-activated LX2 cells (Fig. 2D). Besides, the levels of HSC activation-related markers (including α-SMA and Col1A1) were measured by western blot. It was found that hsa_circ_0072765 deficiency decreased the protein levels of α-SMA and Col1A1 in TGF-β1-stimulated LX2 cells, indicating the inhibition of HSC activation after hsa_circ_0072765 deficiency (Fig. 2E). Wound-healing assay indicated that hsa_circ_0072765 deficiency restrained the migration of TGF-β1-stimulated LX2 cells (Fig. 2F). Taken together, hsa_circ_0072765 knockdown inhibited TGF-β1-treated HSC proliferation, activation and migration.

Hsa_circ_0072765 directly targeted miR-197-3p

By searching circinteractome (https://circ

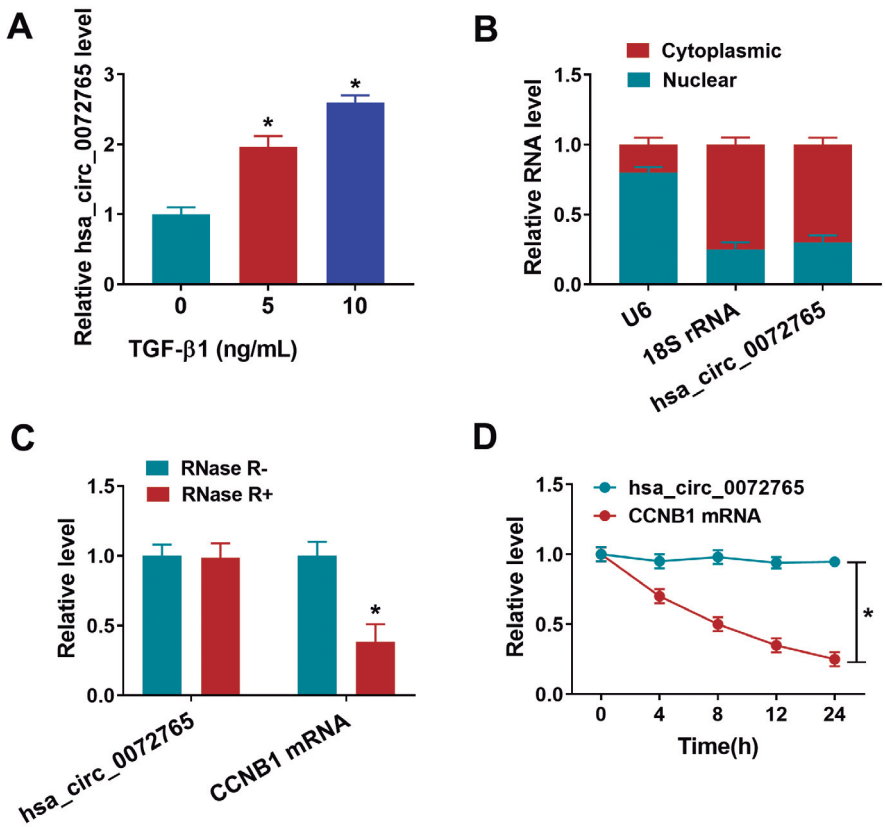

Fig. 1. Hsa_circ_0072765 was highly expressed in TGF-β1-treated HSCs. **A.** The expression of hsa_circ_0072765 in TGF-β1-treated LX2 cells was determined by qRT-PCR. **B.** The expression of hsa_circ_0072765 in the cytoplasm and nucleus of LX2 cells was detected by qRT-PCR. **C.** The expression of hsa_circ_0072765 and CCNB1 in LX2 cells treated with or without RNase R was detected by qRT-PCR. **D.** After LX2 cells were exposed to Actinomycin D for 0h, 4h, 8h, 12h and 24h, the levels of hsa_circ_0072765 and CCNB1 were examined by qRT-PCR. **P*<0.05.

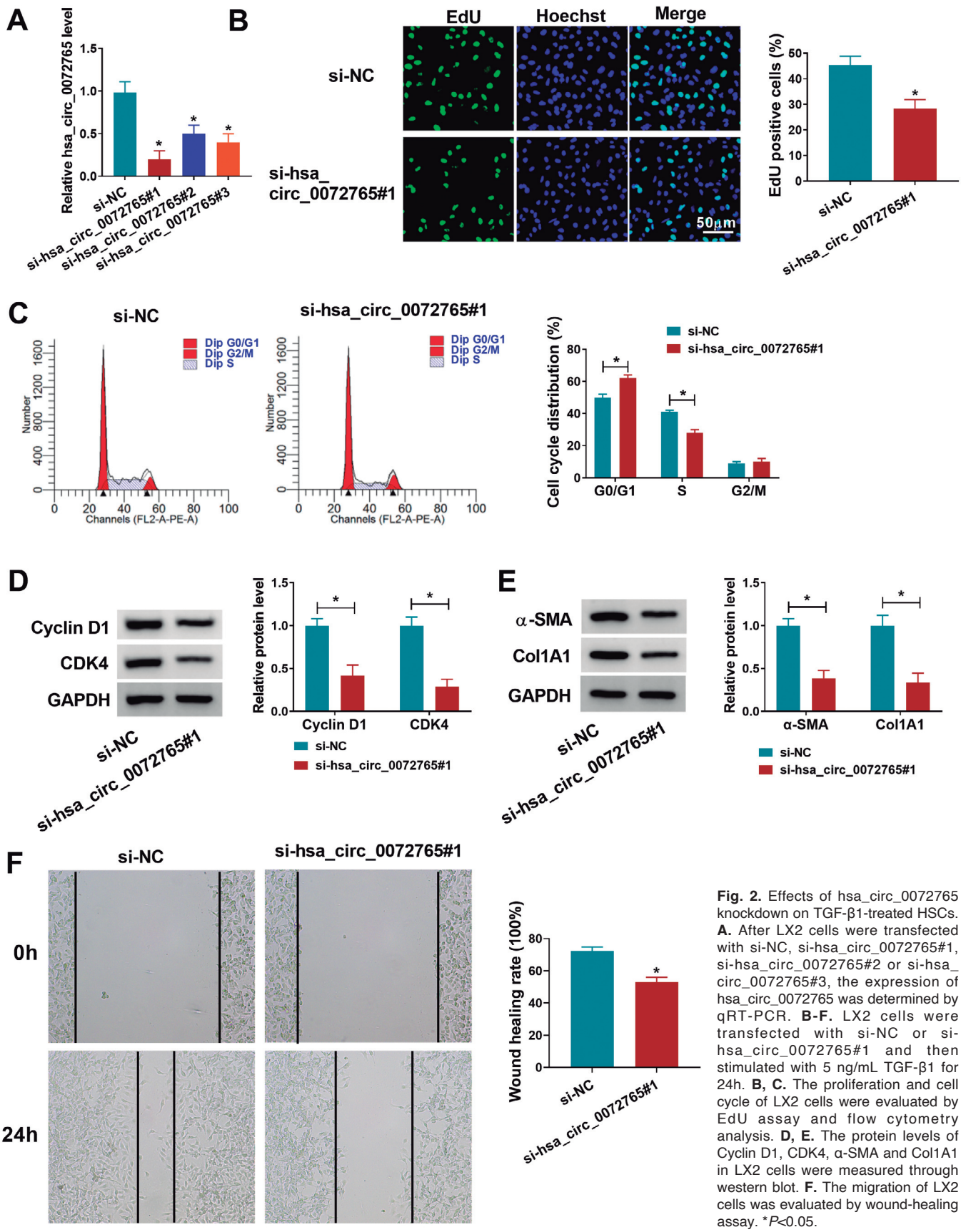

Fig. 2. Effects of hsa_circ_0072765 knockdown on TGF-β1-treated HSCs. **A.** After LX2 cells were transfected with si-NC, si-hsa_circ_0072765#1, si-hsa_circ_0072765#2 or si-hsa_circ_0072765#3, the expression of hsa_circ_0072765 was determined by qRT-PCR. **B-F.** LX2 cells were transfected with si-NC or si-hsa_circ_0072765#1 and then stimulated with 5 ng/mL TGF-β1 for 24h. **B, C.** The proliferation and cell cycle of LX2 cells were evaluated by EdU assay and flow cytometry analysis. **D, E.** The protein levels of Cyclin D1, CDK4, α-SMA and Col1A1 in LX2 cells were measured through western blot. **F.** The migration of LX2 cells was evaluated by wound-healing assay. **P*<0.05.

interactome.nia.nih.gov/api/v2/mirnasearch?circular_rna_query=hsa_circ_0072765&mirna_query=hsa-miR-197&submit=miRNA+Target+Search), miR-197-3p was found to contain the complementary sequences of hsa_circ_0072765 (Fig. 3A). Then the relation between hsa_circ_0072765 and miR-197-3p was further investigated. As indicated by dual-luciferase reporter assay, miR-197-3p overexpression led to the reduction of hsa_circ_0072765-wt luciferase activity in LX2 cells, but did not affect hsa_circ_0072765-mut luciferase activity (Fig. 3B). RIP assay showed that the levels of hsa_circ_0072765 and miR-197-3p were enriched by Anti-Ago2 RIP compared to Anti-IgG control group (Fig. 3C). These results further demonstrated the combination between hsa_circ_0072765 and miR-197-3p. As shown in Fig. 3D, the transfection of hsa_circ_0072765 overexpression vector resulted in the upregulation of hsa_circ_0072765 in LX2 cells. Of note, hsa_circ_0072765 overexpression decreased miR-197-3p expression in LX2 cells, while hsa_circ_0072765 knockdown increased miR-197-3p expression in LX2 cells (Fig. 3E). Collectively, hsa_circ_0072765 negatively regulated miR-197-3p by targeting miR-197-3p.

MiR-197-3p inhibition reversed the effects of hsa_circ_0072765 knockdown on TGF-β1-treated HSC proliferation, cell cycle, activation and migration

Compared to control LX2 cells, miR-197-3p level was weakly expressed in TGF-β1-stimulated LX2 cells (Fig. 4A). As presented in Fig. 4B, anti-miR-197-3p transfection reduced miR-197-3p expression in LX2 cells. To explore the relation between hsa_circ_0072765 and miR-197-3p in TGF-β1-stimulated LX2 cell progression, TGF-β1-stimulated LX2 cells were transfected with si-NC, si-hsa_circ_0072765#1, si-hsa_circ_0072765#1+anti-NC or si-hsa_circ_0072765#1+anti-miR-197-3p. qRT-PCR assay showed that the upregulation of miR-197-3p in TGF-β1-treated LX2 cells mediated by hsa_circ_0072765 knockdown was rescued after anti-miR-197-3p transfection (Fig. 4C). As illustrated by EdU assay and flow cytometry analysis, hsa_circ_0072765 knockdown repressed cell proliferation and cell cycle process in TGF-β1-stimulated LX2 cells, whereas miR-197-3p inhibition abrogated the effects (Fig. 4D,E). Silencing of hsa_circ_0072765 reduced Cyclin D1 and CDK4 levels in TGF-β1-treated LX2 cells, while miR-197-3p downregulation ameliorated the effects (Fig. 4F). The effects of hsa_circ_0072765 silencing on the mRNA and protein levels of HSC activation markers (α-SMA and Col1A1) were also abated by decreasing miR-197-3p (Fig. 4G,H). Besides, hsa_circ_0072765 interference repressed the migration of TGF-β1-treated LX2 cells, while miR-197-3p inhibition weakened the impact (Fig. 4I). To summarize, hsa_circ_0072765 regulated TGF-β1-induced HSC cell proliferation, cell cycle, activation and migration by targeting miR-197-3p.

TRPV3 was the target gene of miR-197-3p

Subsequently, the potential target gene of miR-197-3p was investigated. As analyzed by targetscan (http://www.targetscan.org/cgi-bin/targetscan/vert_71/view_gene.cgi?rs=ENST00000301365.4&taxid=9606&members=miR-197-3p&showcnc=1&shownc=1&shownc_nc=1&showncf1=1&subset=1), TRPV3 was

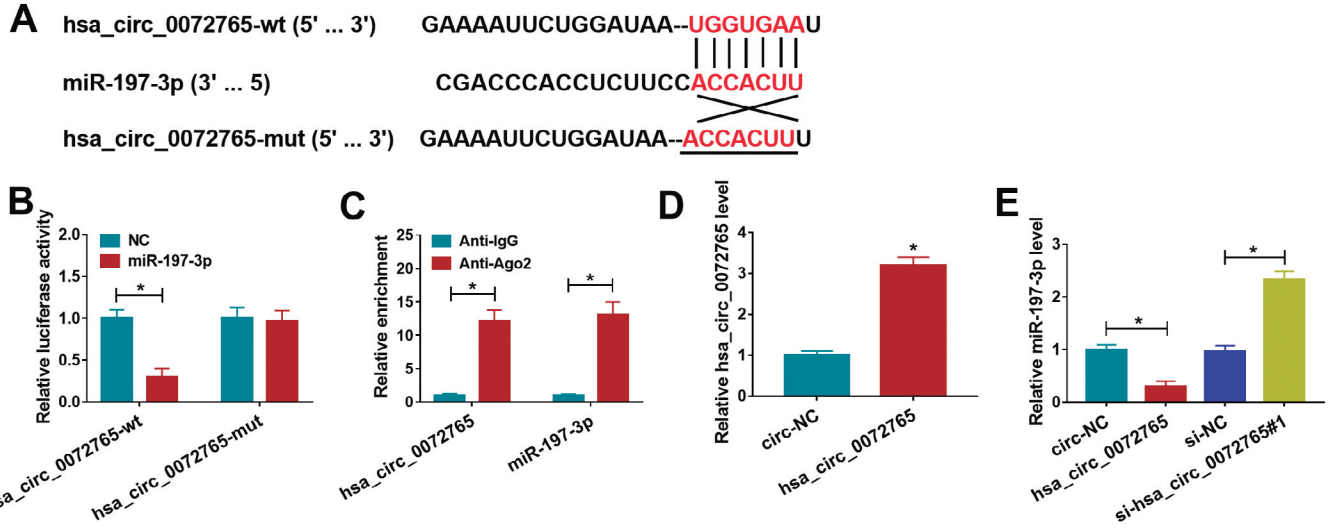

Fig. 3. MiR-197-3p was targeted by hsa_circ_0072765. **A.** Hsa_circ_0072765 contained miR-197-3p binding sites. **B, C.** The association between hsa_circ_0072765 and miR-197-3p was analyzed by dual-luciferase reporter assay and RIP assay. **D.** The expression of hsa_circ_0072765 in LX2 cells transfected with circ-NC or hsa_circ_0072765 was determined by qRT-PCR. **E.** The expression of miR-197-3p in LX2 cells transfected with circ-NC, hsa_circ_0072765, si-NC or si-hsa_circ_0072765#1 was examined by qRT-PCR. *P<0.05.

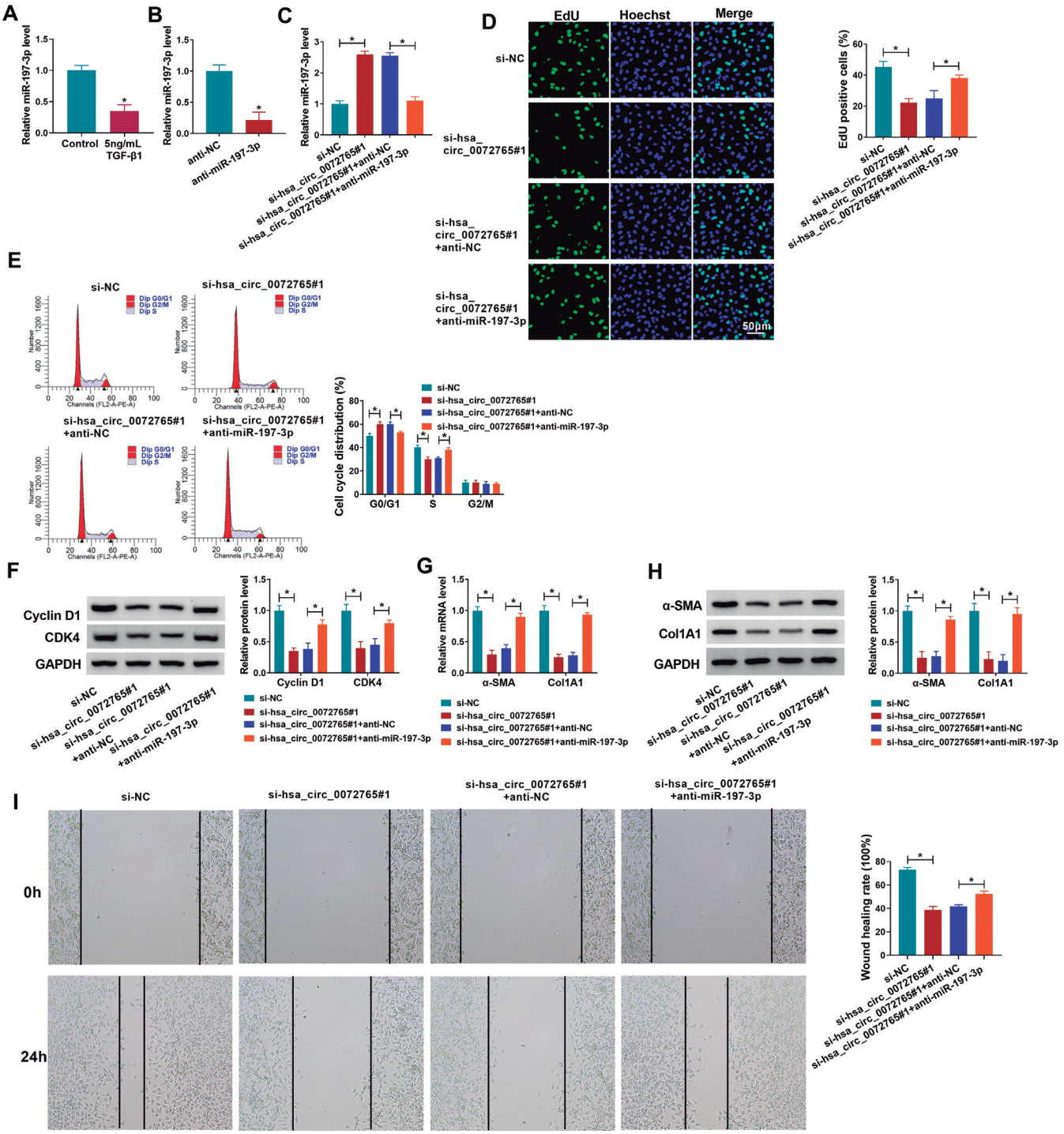

Fig. 4. Hsa_circ_0072765 knockdown repressed cell proliferation, cell cycle, activation and migration in TGF-β1-induced HSC cells by sponging miR-197-3p. **A.** The expression of miR-197-3p in TGF-β1-treated LX2 cells was determined by qRT-PCR. **B.** The expression of miR-197-3p in anti-NC or anti-miR-197-3p transfected LX2 cells was determined by qRT-PCR. **C-H.** TGF-β1-treated LX2 cells were transfected with si-NC, si-hsa_circ_0072765#1, si-hsa_circ_0072765#1+anti-NC or si-hsa_circ_0072765#1+anti-miR-197-3p. **C.** MiR-197-3p expression in LX2 cells was detected by qRT-PCR. **D, E.** The proliferation and cell cycle of LX2 cells were examined by EdU assay and flow cytometry analysis, respectively. **F.** The protein levels of Cyclin D1 and CDK4 were determined by western blot. **G, H.** The mRNA and protein levels of α-SMA and Col1A1 in LX2 cells were measured by qRT-PCR and western blot. **I.** The migration of LX2 cells was evaluated by wound-healing assay. **P*<0.05.

the target gene of miR-197-3p (Fig. 5A). Dual-luciferase reporter assay showed that the luciferase activity of TRPV3-wt was reduced after co-transfection with miR-197-3p in LX2 cells, but the luciferase activity of TRPV3-mut was not affected (Fig. 5B). RIP assay results showed that the enrichments of miR-197-3p and TRPV3 were increased in the Anti-Ago2 group compared to Anti-IgG control group, further confirming the interaction between TRPV3 and miR-197-3p (Fig. 5C). As presented in Fig. 5D, miR-197-3p mimic transfection increased miR-197-3p expression in LX2 cells. Overexpression of hsa_circ_0072765 promoted TRPV3 protein level in LX2 cells, while miR-197-3p mimic transfection ameliorated the effect (Fig. 5E). Furthermore, hsa_circ_0072765 knockdown decreased TRPV3 protein level in LX2 cells, while miR-197-3p inhibition reversed the effect (Fig. 5F). All these results suggested that hsa_circ_0072765 positively modulated TRPV3 expression by targeting miR-197-3p.

MiR-197-3p overexpression inhibited cell proliferation, cell cycle, activation and migration in TGF-β1-activated LX2 cells by targeting TRPV3

As shown in Figure 6A, TRPV3 protein level in LX2 cells was induced by TGF-β1 treatment. After transfected with TRPV3 overexpression vector into LX2 cells, TRPV3 protein level was markedly increased (Fig. 6B). Next, whether miR-197-3p could regulate TGF-β1-induced LX2 cell progression was investigated. The results in Figure 6C showed that miR-197-3p overexpression decreased TRPV3 protein level in TGF-β1-treated LX2 cells, whereas the effect was rescued by transfecting TRPV3 overexpression vector. EdU assay and flow cytometry analysis indicated that miR-197-3p overexpression restrained cell proliferation and arrested cell cycle in TGF-β1-treated LX2 cells, but the effects were abated by upregulating TRPV3 (Fig. 6D,E). MiR-197-3p overexpression decreased the protein levels of Cyclin D1 and CDK6, as well as the mRNA and protein levels of α-SMA and Col1A1 in TGF-β1-treated LX2 cells, while TRPV2 elevation rescued the effects (Fig. 6F-H). In addition, wound-healing assay indicated that miR-197-3p overexpression suppressed the migration of TGF-β1-treated LX2 cells, while the effect was overturned by elevating TRPV3 (Fig. 6I). Taken together, miR-197-3p overexpression repressed TGF-β1-treated LX2 cell progression by targeting TRPV3.

Exosomal hsa_circ_0072765 was increased in TGF-β1-treated LX2 cells

The exosomes were extracted from LX2 cells with or without (control) TGF-β1 treatment. The exosomes showed the typical cup-shaped vesicles (Fig. 7A). Moreover, the exosome markers CD9 and CD63 could be detected in the exosomes isolated from TGF-β1-treated LX2 cells and control cells (Fig. 7B).

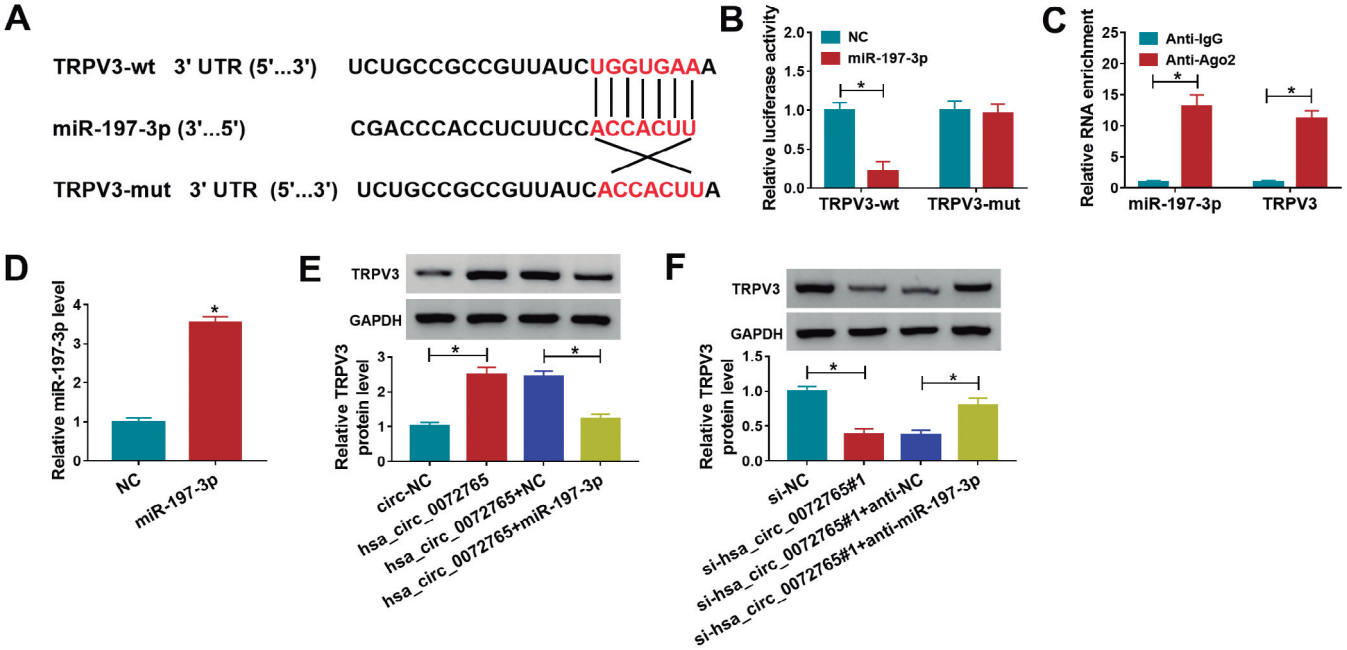

Fig. 5. MiR-197-3p interacted with TRPV3. **A.** TRPV3 contained miR-197-3p binding sites. **B, C.** The relationship between miR-197-3p and TRPV3 was analyzed by dual-luciferase reporter assay and RIP assay. **D.** The expression of miR-197-3p in LX2 cells transfected with NC or miR-197-3p was determined by qRT-PCR. **E, F.** After LX2 cells were transfected with circ-NC, hsa_circ_0072765, hsa_circ_0072765+NC, hsa_circ_0072765+miR-197-3p, si-NC, si-hsa_circ_0072765#1, si-hsa_circ_0072765#1+anti-NC or si-hsa_circ_0072765#1+anti-miR-197-3p, the protein level of TRPV3 in LX2 cells was measured via western blot. *P<0.05.

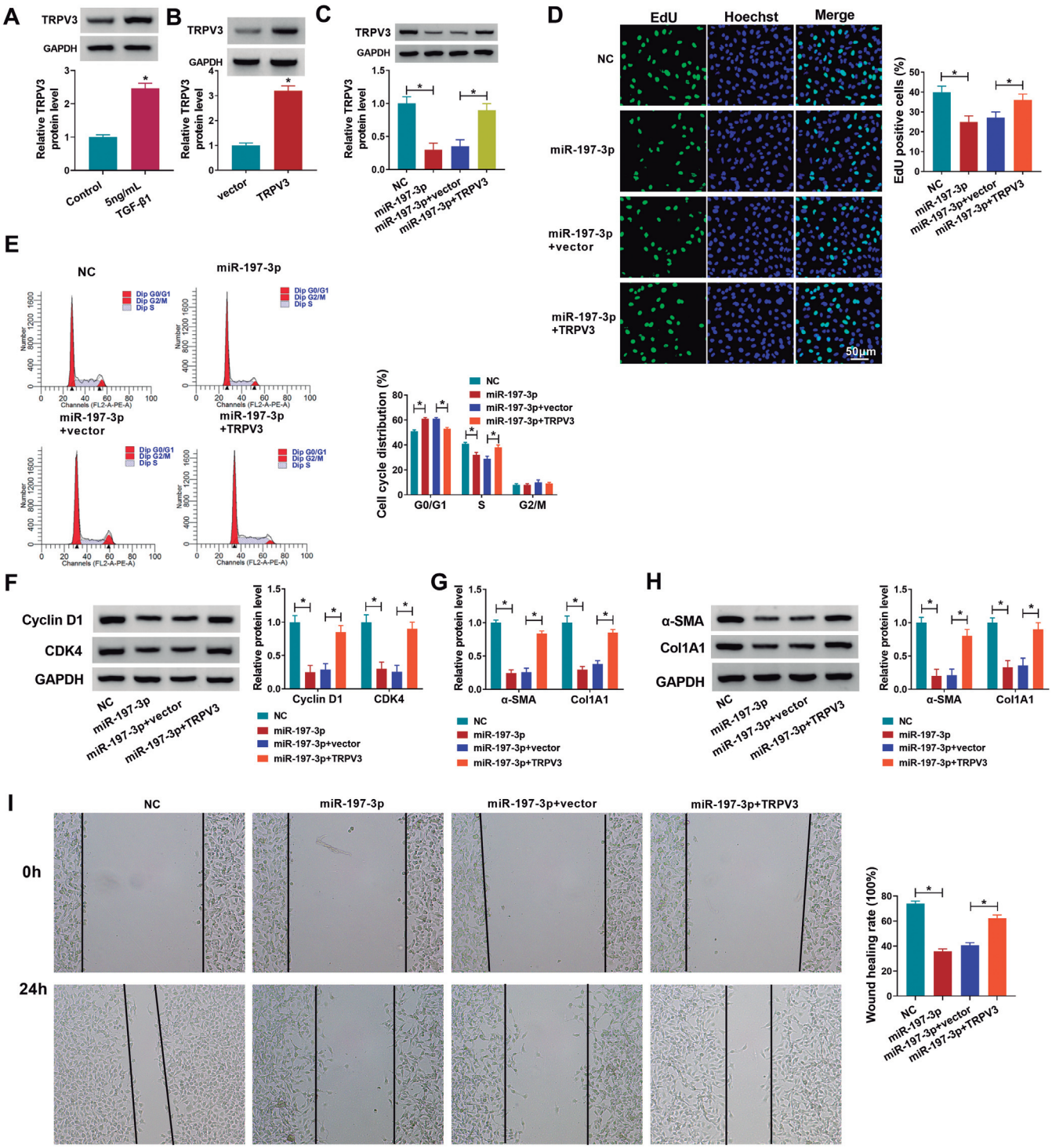

Fig. 6. MiR-197-3p overexpression restrained TGF-β1-activated LX2 cell proliferation, cell cycle, activation and migration by targeting TRPV3. **A.** The protein of TRPV3 in TGF-β1-treated LX2 cells was measured by western blot. **B.** The protein level of TRPV3 in LX2 cells transfected with vector or TRPV3 was examined by western blot. **C-H.** TGF-β1-treated LX2 cells were transfected with NC, miR-197-3p, miR-197-3p+vector or miR-197-3p+TRPV3. **C.** TRPV3 protein level in LX2 cells was detected by western blot. **D, E.** LX2 cell proliferation and cell cycle process were estimated by EdU assay and flow cytometry analysis. **F.** The protein levels of Cyclin D1 and CDK6 in LX2 cells were measured via western blot. **G, H.** The mRNA and protein levels of α-SMA and Col1A1 in LX2 cells were examined by qRT-PCR and western blot. **I.** The migration of LX2 cells was evaluated by wound-healing assay. **P*<0.05

Hsa_circ_0072765 level was increased in the exosomes derived from TGF-β1-treated LX2 cells (Fig. 7C). Then, LX2 cells were incubated with TGF-β1-treated LX2 cell-derived exosomes and we found that hsa_circ_0072765 level was increased after the incubation (Fig. 7D). Furthermore, the treatment of exosome inhibitor GW4869 reduced hsa_circ_0072765 level in TGF-β1-treated LX2 cells (Fig. 7E).

Discussion

Liver fibrosis is a dynamic, highly debilitating pathology caused by continuous wound healing during chronic liver injury. HSCs play a vital role in liver fibrosis because of their ability to produce fibrotic proteins, such as α-SMA and CoL1A1 (Hernandez-Gea and Friedman, 2011; Parola and Pinzani, 2019). During HSC activation, the pro-fibrogenic cytokine TGF-β1 was released and contributed to liver fibrosis (Fouts et al., 2012; Yu et al., 2019). Thus, we treated HSCs with TGF-β1 to mimic liver fibrosis cell model *in vitro*. According to our results, we believe that hsa_circ_0072765 knockdown may be an effective measure to alleviate liver fibrosis. Our data indicated that targeting the hsa_circ_0072765/miR-197-3p/TRPV3 regulatory axis may provide new ideas for the treatment of liver fibrosis.

Recently, circRNAs have been reported to play crucial roles in liver fibrosis. CircCMOT1 repressed the activation of HSCs by altering miR-181b-5p and PTEN (Jin et al., 2020). Hsa_circ_0004018 was weakly expressed in liver fibrogenesis and restrained HSC proliferation and activation by enhancing miR-660-3p-dependent TEP1 expression (Li et al., 2020). Though several circRNAs have been identified in liver fibrosis development, the functions of hsa_circ_0072765 are still unclear. Herein, hsa_circ_0072765 was elevated in TGF-β1-activated HSCs. Silencing of hsa_circ_0072765 suppressed cell proliferation, cell cycle and migration in TGF-β1-treated HSCs. Moreover, we determined the levels of fibrogenic proteins α-SMA and Col1A1 in TGF-β1-activated HSCs. Our results showed that hsa_circ_0072765 interference reduced the levels of α-SMA and Col1A1, indicating the inhibition of HSC activation.

Subsequently, hsa_circ_0072765 was demonstrated to decoy miR-197-3p to alter miR-197-3p expression. MiR-197-3p served as an essential regulator in multiple diseases, such as kawasaki disease (Liu et al., 2021), cervical cancer (Gu et al., 2021) and prostate cancer (Huang et al., 2020). In this study, we elucidated the roles of miR-197-3p in TGF-β1-treated HSC progression. As a result, miR-197-3p enhancement reduced TGF-β1-activated HSC proliferation, activation and migration. Moreover, hsa_circ_0072765 modulated TGF-β1-treated HSC progression inhibiting miR-197-3p expression.

MiRNAs can regulate target gene expression by binding to the 3'UTR of target mRNAs (Jansson and Lund, 2012; Tafrihi and Hasheminasab, 2019). Herein, TRPV3 was discovered to be the target gene of miR-

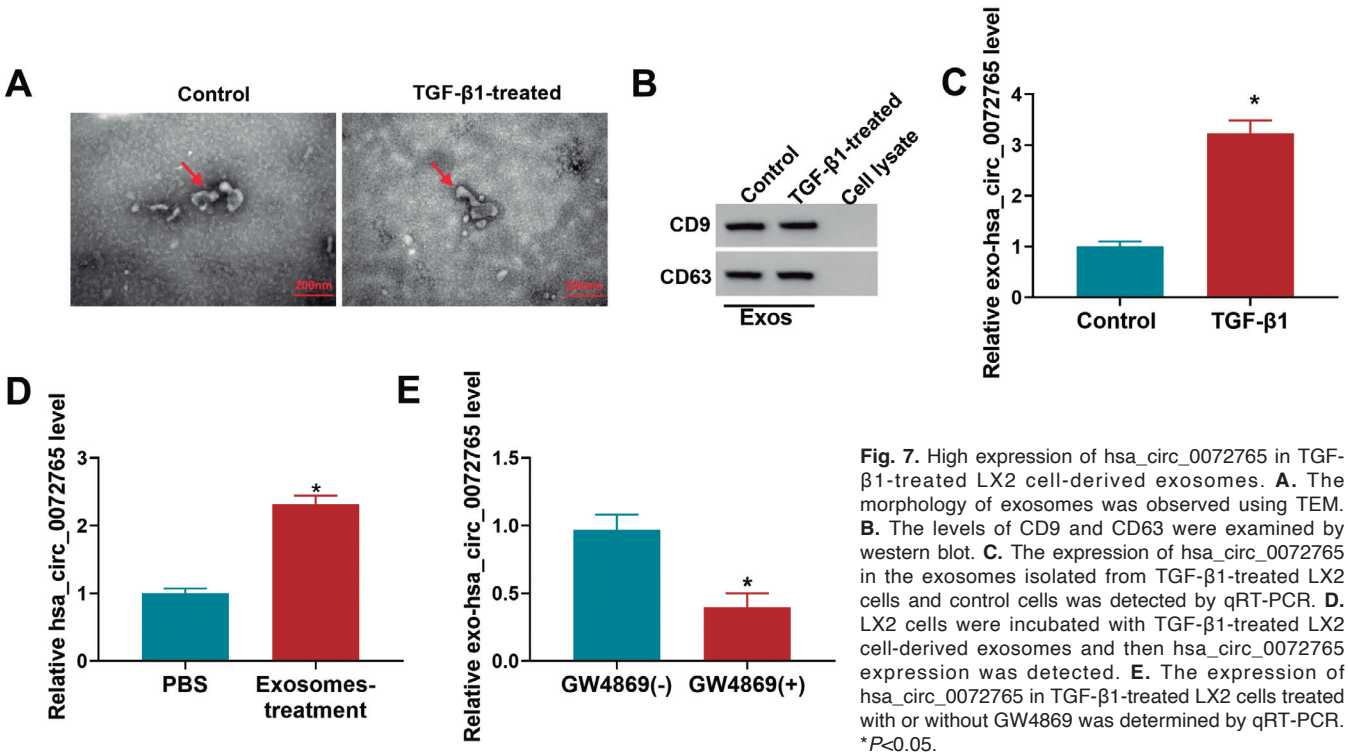

Fig. 7. High expression of hsa_circ_0072765 in TGF-β1-treated LX2 cell-derived exosomes. **A.** The morphology of exosomes was observed using TEM. **B.** The levels of CD9 and CD63 were examined by western blot. **C.** The expression of hsa_circ_0072765 in the exosomes isolated from TGF-β1-treated LX2 cells and control cells was detected by qRT-PCR. **D.** LX2 cells were incubated with TGF-β1-treated LX2 cell-derived exosomes and then hsa_circ_0072765 expression was detected. **E.** The expression of hsa_circ_0072765 in TGF-β1-treated LX2 cells treated with or without GW4869 was determined by qRT-PCR. *P<0.05.

197-3p. TRPV3 belongs to the TRP superfamily and has been demonstrated to exacerbate the development of liver fibrosis (Yan et al., 2021). We found that TRPV3 expression was increased in HSCs after TGF-β1 stimulation. In addition, TRPV3 overexpression promoted miR-197-3p-mediated cell proliferation, activation and migration in TGF-β1-stimulated HSCs.

Exosomes are small extracellular vesicles and are involved in intercellular communication by secreting lipids, lncRNAs, circRNAs, miRNAs and proteins (Santos et al., 2016; Sun et al., 2016).

In summary, hsa_circ_0072765 contributed to cell proliferation, activation and migration in TGF-β1-induced HSCs by elevating TRPV3 through decoying miR-197-3p. The study might provide a reference for the therapy of fibrosis. However, the results still needed to be verified through *in vivo* experiments.

Acknowledgements. None.
Disclosure of interest. The authors declare that they have no conflict of interest.
Funding. None.

References

Barnett R. (2018). Liver cirrhosis. Lancet 392, 275.

Beermann J., Piccoli M.T., Viereck J. and Thum T. (2016). Non-coding RNAs in development and disease: Background, mechanisms, and therapeutic approaches. Physiol. Rev. 96, 1297-1325.

Cabral B.C.A., Hoffmann L., Bottaro T., Costa P.F., Ramos A.L.A., Coelho H.S.M., Villela-Nogueira C.A., Urmenyi T.P., Faffe D.S. and Silva R. (2020). Circulating microRNAs associated with liver fibrosis in chronic hepatitis C patients. Biochem. Biophys. Rep. 24, 100814.

Chen S.N., Chang R., Lin L.T., Chern C.U., Tsai H.W., Wen Z.H., Li Y.H., Li C.J. and Tsui K.H. (2019). MicroRNA in ovarian cancer: Biology, pathogenesis, and therapeutic opportunities. Int. J. Environ. Res. Public. Health 16, 1510.

Cong S., Liu Y., Li Y., Chen Y., Chen R., Zhang B., Yu L., Hu Y., Zhao X., Mu M., Cheng M. and Huang Z. (2021). MiR-571 affects the development and progression of liver fibrosis by regulating the Notch3 pathway. Sci. Rep. 11, 21854.

Esteller M. (2011). Non-coding RNAs in human disease. Nat. Rev. Genet. 12, 861-874.

Fouts D.E., Torralba M., Nelson K.E., Brenner D.A. and Schnabl B. (2012). Bacterial translocation and changes in the intestinal microbiome in mouse models of liver disease. J. Hepatol. 56, 1283-1292.

Friedman S.L. (2008). Hepatic stellate cells: protean, multifunctional, and enigmatic cells of the liver. Physiol. Rev. 88, 125-172.

Gu Q., Hou W., Shi L., Liu H., Zhu Z. and Ye W. (2021). Circular RNA ZNF609 functions as a competing endogenous RNA in regulating E2F transcription factor 6 through competitively binding to microRNA-197-3p to promote the progression of cervical cancer progression. Bioengineered 12, 927-936.

Hernandez-Gea V. and Friedman S.L. (2011). Pathogenesis of liver fibrosis. Annu. Rev. Pathol. 6, 425-456.

Huang Q., Ma B., Su Y., Chan K., Qu H., Huang J., Wang D., Qiu J., Liu H., Yang X. and Wang Z. (2020). miR-197-3p represses the proliferation of prostate cancer by regulating the VDAC1/AKT/beta-catenin signaling axis. Int. J. Biol. Sci. 16, 1417-1426.

Jansson M.D. and Lund A.H. (2012). MicroRNA and cancer. Mol. Oncol. 6, 590-610.

Jin H., Li C., Dong P., Huang J., Yu J. and Zheng J. (2020). Circular RNA cMTO1 promotes PTEN expression through sponging miR-181b-5p in liver fibrosis. Front. Cell Dev. Biol. 8, 714.

Li S., Song F., Lei X., Li J., Li F. and Tan H. (2020). hsa_circ_0004018 suppresses the progression of liver fibrosis through regulating the hsa-miR-660-3p/TEP1 axis. Aging (Albany. NY) 12, 11517-11529.

Liu W., Feng R., Li X., Li D. and Zhai W. (2019). TGF-beta- and lipopolysaccharide-induced upregulation of circular RNA PWWP2A promotes hepatic fibrosis via sponging miR-203 and miR-223. Aging (Albany. NY) 11, 9569-9580.

Liu C., Yang D., Wang H., Hu S., Xie X., Zhang L., Jia H. and Qi Q. (2021). MicroRNA-197-3p mediates damage to human coronary artery endothelial cells via targeting TIMP3 in Kawasaki disease. Mol. Cell. Biochem. 476, 4245-4263.

Lu L.G., Zeng M.D., Wan M.B., Li C.Z., Mao Y.M., Li J.Q., Qiu D.K., Cao A.P., Ye J., Cai X., Chen C.W., Wang J.Y., Wu S.M., Zhu J.S. and Zhou X.Q. (2003). Grading and staging of hepatic fibrosis, and its relationship with noninvasive diagnostic parameters. World J. Gastroenterol. 9, 2574-2578.

Luersen G.F., Bhosale P. and Szklaruk J. (2015). State-of-the-art cross-sectional liver imaging: beyond lesion detection and characterization. J. Hepatocell. Carcinoma 2, 101-117.

Matsuda M., Tsurusaki S., Miyata N., Saijou E., Okochi H., Miyajima A. and Tanaka M. (2018). Oncostatin M causes liver fibrosis by regulating cooperation between hepatic stellate cells and macrophages in mice. Hepatology 67, 296-312.

Ninomiya M., Kondo Y., Funayama R., Nagashima T., Kogure T., Kakazu E., Kimura O., Ueno Y., Nakayama K. and Shimosegawa T. (2013). Distinct microRNAs expression profile in primary biliary cirrhosis and evaluation of miR 505-3p and miR197-3p as novel biomarkers. PLoS One 8, e66086.

Parola M. and Pinzani M. (2019). Liver fibrosis: Pathophysiology, pathogenetic targets and clinical issues. Mol. Aspects Med. 65, 37-55.

Salzman J. (2016). Circular RNA expression: its potential regulation and function. Trends Genet. 32, 309-316.

Santos J.C., Ribeiro M.L., Sarian L.O., Ortega M.M. and Derchain S.F. (2016). Exosomes-mediate microRNAs transfer in breast cancer chemoresistance regulation. Am. J. Cancer Res. 6, 2129-2139.

Sun L., Xu R., Sun X., Duan Y., Han Y., Zhao Y., Qian H., Zhu W. and Xu W. (2016). Safety evaluation of exosomes derived from human umbilical cord mesenchymal stromal cell. Cytotherapy 18, 413-422.

Tafrihi M. and Hasheminasab E. (2019). MiRNAs: Biology, biogenesis, their web-based tools, and databases. MicroRNA 8, 4-27.

Vishnoi A. and Rani S. (2017). MiRNA biogenesis and regulation of diseases: An overview. Methods Mol. Biol. 1509, 1-10.

Wang A., Bu F.T., Li J.J., Zhang Y.F., Jia P.C., You H.M., Wu S., Wu Y.Y., Zhu S., Huang C. and Li J. (2021). MicroRNA-195-3p promotes hepatic stellate cell activation and liver fibrosis by suppressing PTEN expression. Toxicol. Lett. 355, 88-99.

Yan L., Zhang X., Fu J., Liu Q., Lei X., Cao Z., Zhang J., Shao Y., Tong Q., Qin W., Liu X., Liu C., Liu Z., Li Z., Lu J. and Xu X. (2021). Inhibition of the transient receptor potential vanilloid 3 channel attenuates carbon tetrachloride-induced hepatic fibrosis. Biochem. Biophys. Res. Commun. 558, 86-93.

Yang G., Li X., Liu J., Huang S., Weng Y., Zhu J., Lin D. and Jiang O. (2021). Hsa_circ_0008537 facilitates liver carcinogenesis by upregulating MCL1 and Snail1 expression via miR1533p. Oncol. Rep. 45, 1072-1082.

Yu H.X., Yao Y., Bu F.T., Chen Y., Wu Y.T., Yang Y., Chen X., Zhu Y., Wang Q., Pan X.Y., Meng X.M., Huang C. and Li J. (2019). Blockade of YAP alleviates hepatic fibrosis through accelerating apoptosis and reversion of activated hepatic stellate cells. Mol. Immunol. 107, 29-40.

Yu M.C., Ding G.Y., Ma P., Chen Y.D., Zhu X.D., Cai J.B., Shen Y.H., Zhou J., Fan J., Sun H.C., Kuang M. and Huang C. (2021). CircRNA UBAP2 serves as a sponge of miR-1294 to increase tumorigenesis in hepatocellular carcinoma through regulating c-Myc expression. Carcinogenesis. 42, 1293-1303.

Zeng X., Yuan X., Cai Q., Tang C. and Gao J. (2021). Circular RNA as an epigenetic regulator in chronic liver diseases. Cells 10, 1945.

Accepted January 17, 2023